Available online at www.sciencedirect.com

ScienceDirect

journal homepage: www.elsevier.com/locate/he

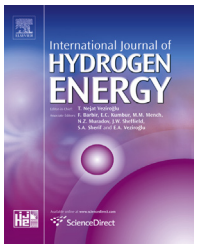

Nickel/gadolinium-doped ceria anode for direct ethanol solid oxide fuel cell

Bruno L. Augusto [a,b], Fábio B. Noronha [b], Fabio C. Fonseca [c], Francisco N. Tabuti [c], Rita C. Colman [a], Lisiane V. Mattos [a,*]

[a] Universidade Federal Fluminense, Rua Passo da Pátria, 156, Niterói, Rio de Janeiro, CEP 24210-240, Brazil
[b] Instituto Nacional de Tecnologia – INT, Av. Venezuela 82, CEP 20081-312, Rio de Janeiro, Brazil
[c] Instituto de Pesquisas Energéticas e Nucleares, IPEN-CNEN/SP, 05508-000, São Paulo, Brazil

ARTICLE INFO

Article history:
Received 30 March 2014
Received in revised form
11 May 2014
Accepted 14 May 2014
Available online 13 June 2014

Keywords:
Hydrogen production
Solid oxide fuel cell
Steam reforming of ethanol
Ni/ gadolinia-doped ceria

ABSTRACT

This report investigates the properties of nickel/gadolinium-doped ceria (Ni/GDC) as anode material for bio-ethanol fueled SOFC. The Ni/GDC cermets with 18 and 44 wt.% Ni were prepared by a hydrothermal method. Ethanol decomposition, steam reforming, and partial oxidation of ethanol were studied using a fixed-bed reactor at 1123 K. Carbon was formed only under dry ethanol for both catalysts. The addition of water or oxygen to the feed inhibited the formation of carbon. Ni/GDC was used as the anode current collector layer and as a catalytic layer in single cells tests. No deposits of carbon were detected in single cells with Ni/GDC catalytic layer after 50 h of continuous operation under direct (dry) ethanol. This result was attributed to the catalytic properties of the Ni/GDC layer and the operation mechanism of gradual internal reforming, in which the oxidation of hydrogen provides the steam for ethanol reforming, thus avoiding carbon deposition.

Introduction

Solid oxide fuel cell (SOFC) technology is considered a promising alternative to provide clean electric power. Advantages include high efficiency, relatively low sensitivity to impurities, and the possibility of operating with an internal reformer [1–3]. In the case of direct internal reforming solid oxide fuel cells (DIR-SOFC), the complexity and costs of the fuel cell system are reduced, since the available fuels (hydrocarbons or alcohols) can be fed straight to the anode and reformed to H_2 and CO without the need of an external reformer. In addition, the conversion of these fuels at the anode side can be promoted due to H_2 consumption by the electrochemical reaction, leading to higher conversions and higher efficiencies [1,4,5]. Bio-ethanol is an attractive alternative renewable fuel that can be produced from a variety of biomass sources (e.g., fermentation of sugar cane, fermentation of corn grains, agricultural wastes, and forestry residues) and does not contribute to net CO_2 emissions. Furthermore, in countries like Brazil and the USA, the ethanol production and distribution infrastructures are already established.

Thus, ethanol is an efficient and available fuel that can play an important role as a carbon neutral fuel for SOFC. Nonetheless, relatively few studies have reported on bio-ethanol fueled SOFC. In fact, most of the reported results concern

* *Corresponding author*. Tel.: +55 21 2629 5599; fax: +55 21 2629 5429.
E-mail addresses: lisiane@vm.uff.br, lisianemattos@yahoo.com.br (L.V. Mattos).
http://dx.doi.org/10.1016/j.ijhydene.2014.05.088

ethanol-water mixtures as fuel [6–11], while a limited number of studies have investigated the direct use of pure (dry) ethanol [12–17]. Moreover, data on the stability of such single cells over reasonable periods of time are seldom found [7,16,17].

Different materials have been used as anodes for ethanol fueled SOFC systems. Ni/yttria-stabilized zirconia (Ni/YSZ) cermets are the standard anodes of SOFC systems [18–20]. Ni provides electronic conductivity, while YSZ provides ionic conductivity and thermal stability. However, in order to exceed the percolation threshold for electronic conductivity, a high Ni content (>30 vol. %) is necessary. Since Ni is very active to reforming as well as cracking reactions, such a high volumetric fraction favors carbon formation when hydrocarbons or bio-ethanol are fed directly in SOFCs. The carbon deposits on metal sites located on the anode resulting in rapid degradation of the fuel cell [18,19]. Significant carbon deposition has been detected on Ni/YSZ anodes of SOFC containing high Ni loading and operating directly on pure ethanol [1]. Therefore, the development of anodes for direct ethanol SOFCs that exhibit high catalytic activity to ethanol conversion, high stability and adequate ionic and electronic conductivity at working conditions is still a challenge.

Some strategies have been proposed for suppressing carbon deposition over SOFC anodes such as: (i) the addition of water and/or O_2 to the feed, (ii) the development of alternative anodes, or (iii) the use of catalytic (barrier) layers.

Augusto et al. [21] reported that the addition of water or oxygen to the feed decreases carbon formation during ethanol reforming over Ni/GDC catalysts. Results were explained by a mechanism proposed for the reactions of ethanol conversion over cerium based catalysts [22]. According to this mechanism, carbon formation during ethanol reforming is due to the dehydrogenation of CH_x species, forming C and H. These highly reactive carbon species were formed by the decomposition of dehydrogenated species (e.g., ethoxy, acetaldehyde, acetyl) and acetate species. The oxygen and/or water in the feed can react with these carbon species, producing CO_x species, which avoids catalyst deactivation. Laosiripojana et al. [23] investigated the effect of H_2O/ethanol molar ratio on the amount of carbon formed during steam reforming (SR) of ethanol over Ni/CeO_2 catalysts. Increasing the H_2O/ethanol molar ratio decreased the amount of carbon deposited on the catalysts. However, some researchers [6,11] showed that the use of high steam/ethanol ratios leads to a decrease in the electrical efficiency of the SOFC system.

Alternative materials have been proposed as anodes for SOFC running directly on ethanol such as Cu supported on ceria-based oxides [6,9,12,14,24]. Ceria exhibits a mixed ionic and electronic conductivity under reducing atmosphere with good compatibility with standard SOFC components [25]. In addition, higher conductivities were obtained when ceria was doped with trivalent cations, such as Gd^{3+} [26]. Furthermore, the high oxygen storage capacity of ceria provides a high resistance to carbon deposition during ethanol reforming [27,28]. However, only few studies reported the use of Ni supported on ceria based oxides as anodes of SOFC running on ethanol [13]. Muccillo et al. [13] reported the current–voltage and impedance spectroscopy measurements for SOFC running directly on ethanol, using a commercial Ni/GDC anode (45 vol. %). The results obtained showed a strong deactivation of these anodes at high temperatures (>1073 K), which was attributed to the carbon formation. Nonetheless, the characterization of the tested anodes was not shown.

Another possibility for reducing carbon deposition is the use of anodes with low Ni content. Decreasing the metal content leads to the formation of smaller crystallite sizes. Since the initiation step for carbon formation is more difficult for smaller particles, controlling the number of atoms in an ensemble will most likely suppress the rate of coke formation [29]. In addition, the high metal dispersion obtained for metal nanoparticles increases the number of active sites at Ni based anodes, improving the performance of the SOFC [30]. However, cermets with metal contents below 30 vol. % and prepared by conventional methods did not exhibit an appropriate conductivity for SOFC applications [31].

Therefore, some authors [30,31] have proposed the use of alternative methods to prepare Ni-based anodes with high activity, high stability, high conductivity, and low metal content. Jasinski et al. [31] prepared Ni/samarium-doped ceria cermets with low Ni contents (7.5, 11 and 14 vol. %) by a net-shape procedure. They investigated the effect of Ni content on the electrical conductivity of the anodes under air or using a mixture containing 10% of hydrogen. The conductivity of the cermet with 14 vol. % Ni was close to the conductivity of the cermet with 35 vol. % Ni prepared by a conventional technique. In addition, the anode with 14 vol. % Ni was stable under hydrogen during a period of several hours. According to them, the Ni anode prepared by the alternative method exhibited unique properties and does not follow percolation theory. Recently, a hydrothermal method has been used to prepare anodes for SOFC with high resistance to carbon formation. Ni-based anodes with low metal content (5 wt.% Ni and 5 wt.% Ru) prepared by the hydrothermal method did not exhibit carbon formation during oxidative steam reforming (OSR) of propane under SOFC operating conditions [30]. Augusto et al. [21] investigated the performance of Ni/GDC anodes with low Ni content (18 wt.% Ni) prepared by a hydrothermal method for ethanol conversion reactions. The reaction conditions significantly affected the activity and stability of the catalysts. Ethanol decomposition (ED), SR and partial oxidation (POX) of ethanol reactions at 773 and 1073 K were performed. All samples deactivated during reaction under pure ethanol at 773 K. The addition of water or oxygen to the feed and the increase of reaction temperature improved catalyst stability. Scanning electron microscopy (SEM) and thermogravimetric analysis (TG) showed that the deactivation was due to carbon formation. In the presence of oxygen or water, the mechanism of carbon removal was favored. Moreover, carbon formation was not favored at high reaction temperature due to the reverse of the Boudouard reaction as well as the promoting effect of the support on the carbon gasification reaction. However, Modafferi et al. [30] and Augusto et al. [21] did not study the electrochemical properties of fuel cells operating on ethanol.

Alternatively, instead of changing the standard Ni/YSZ anode some studies reported promising results using a catalytic layer. Such an approach avoids the challenges of finding alternative anodes with superior properties than the ones of Ni/YSZ cermets. The main idea is to separate the

electrochemical and catalytic functions of the anode into two layers: the standard anode and a catalytic layer, respectively. The catalytic layer converts the fuel into hydrogen and serves as a physical barrier that avoids the direct contact of the Ni/YSZ cermet and the fuel.

Therefore, the aim of the present study is to study the performance of Ni/GDC as anodes for bio-ethanol fueled SOFCs. Cermets Ni/GDC with 18 and 44 wt.% Ni were prepared by a hydrothermal method. These Ni contents correspond to 14 and 30 vol.% Ni, representative of a low and a conventional Ni content, respectively, for typical SOFC anodes. The structural properties, particle size changes, and the microstructure of the anodes were investigated by X-ray diffraction (XRD) and SEM. The catalytic performance of the samples for ethanol reforming reactions was evaluated, using a conventional fixed-bed reactor at the reaction temperature typical of a DIR-SOFC (1123 K). The electrical conductivity and the properties of the Ni/GDC anodes were investigated in ethanol fueled single cells. Cermets were investigated in two cell configurations: i) conventional electrolyte-supported fuel cell, in which the Ni/GDC was the anode current collector layer (anode outer layer); and ii) fuel cell with a catalytic layer (cathode/electrolyte/anode/catalyst), in which the low Ni-content (18 wt.%) Ni/GDC cermet was deposited onto a Ni/YSZ anode. The later SOFC was continuously operated at 1123 K for ~50 h in order to evaluate its long term stability. After both catalytic and fuel cell tests, TG and SEM analyses were carried out to investigate the carbonaceous deposits formed under various reaction conditions.

Experimental

Catalyst preparation

The GDC support was synthesized by a hydrothermal method previously described elsewhere [30]. An aqueous solution of cerium (IV) ammonium nitrate and gadolinium nitrate was prepared with a Gd/Ce molar ratio of 1/9. Cerium and gadolinium hydroxides were then co-precipitated by the addition of excess of ammonium hydroxide. The precipitate was transferred to an autoclave and heated to 453 K for 4 h. Then, the precipitate was washed with distilled water and calcined at 573 K for 2 h in a muffle furnace (GDC-573). Ni was added to GDC-573 support by wet impregnation using an aqueous solution of $Ni(NO_3).6H_2O$. After impregnation, the sample was dried at 393 K and calcined under air (50 mL/min) at 1473 K according to the following temperature program: (i) from room temperature to 673 K at 0.5 K min^{-1}; (ii) from 673 to 973 K at 1.7 K min^{-1} and (iii) from 973 to 1473 K at 10 K min^{-1}, remaining at the final temperature for 5 h. Two samples containing 18 and 44 wt.% of Ni were prepared (18 Ni/GDC and 44 Ni/GDC, respectively).

X-ray diffraction (XRD)

The X-ray powder diffraction pattern of the calcined and reduced/passivated samples were obtained with CuK_α radiation ($\lambda = 1.5406$ Å) using a RIGAKU diffractometer. Data were collected over the 2θ range of 25°–75° using a scan rate of 0.04°/step and a scan time of 1 s/step. The Scherrer equation was used to estimate the crystallite mean diameters of CeO_2, NiO, and Ni. For the measurements of the crystallite mean diameter of Ni, the calcined samples were also reduced under pure hydrogen (30 mL/min) at 1023 K for 1 h, purged under N_2 at the same temperature for 30 min and cooled to 298 K. Then, the reactor was maintained at 209 K by immersing it in a mixture of isopropyl alcohol and liquid nitrogen for 1 h, and the catalyst was passivated with a 5% O_2/He mixture.

Thermogravimetric analysis (TG)

Temperature programmed oxidation (TPO) experiments were performed using a Shimadzu (TG – 60) instrument in order to determine the amount of carbon formed over the catalyst. The analyses were carried out after ethanol reactions at 773 and 1073 K. For the TPO experiments, the residence time used for each reaction test was selected in order to obtain the same initial ethanol conversion for all samples. Approximately 10 mg of spent catalyst was heated under air flow from room temperature to 1273 K at a heating rate of 20 K/min and the weight change was measured.

Scanning electron microscopy (SEM)

Scanning electron microscopy (SEM) of the fresh, reduced and spent catalysts was carried out using a FEI Inspect S scanning electron microscope equipped with a secondary electron analyzer. The microscope was also equipped with an EDAX analytical system energy dispersive spectrometer (EDS). The samples were reduced following the same conditions previously described in the XRD section.

Conventional fixed-bed reactor (CR)

Direct ethanol decomposition (ED), steam reforming (SR) and partial oxidation (POX) of ethanol were performed using a quartz tube reactor at 1123 K under atmospheric pressure. Prior to reaction, samples were reduced under pure hydrogen (30 mL/min) at 1023 K for 1 h and then purged with N_2 at the same temperature for 30 min. For SR, a stoichiometric H_2O/ethanol molar ratio of 3.0 was used. POX was conducted using an O_2/ethanol molar ratio of 0.5. The reactant mixtures were obtained using two saturators containing water and ethanol, which were maintained at the temperature required to obtain the desired H_2O/ethanol and O_2/ethanol molar ratios. For ED and POX, N_2 (30 mL/min) and 5.6% O_2/N_2 mixture (30 mL/min), respectively, were passed through the saturator with ethanol, and then the reactant mixtures obtained were diluted with N_2 (each N_2 stream flowed at 30 mL/min). In the case of SR, the reactant mixture was obtained by flowing two N_2 streams (30 mL/min) through each saturator containing ethanol and water separately. The partial pressure of ethanol was maintained constant for all experiments.

In order to observe the catalyst deactivation within a short timeframe, a small amount of catalyst was used (20 mg). The samples were diluted with inert SiC (SiC mass/catalyst mass = 3.0). The reaction products were analyzed by gas chromatography (Micro GC Agilent 3000 A) containing three channels for three thermal conductivity detectors (TCD) and

three columns: a molecular sieve, a Poraplot Q and OV-1 column. The ethanol conversion and selectivity to products were determined as follows:

$$X_{ethanol} = \frac{(n_{ethanol})_{fed} - (n_{ethanol})_{exit}}{(n_{ethanol})_{fed}} \times 100 \quad (1)$$

$$S_x = \frac{(n_x)_{produced}}{(n_{total})_{produced}} \times 100 \quad (2)$$

where $(n_x)_{produced}$ = moles of x produced (x = hydrogen, CO, CO_2, methane, acetaldehyde or ethylene) and $(n_{total})_{produced}$ = moles of H_2 + moles of CO + moles of CO_2 + moles of methane + moles of acetaldehyde + moles of ethylene (i.e., the moles of water produced are not included).

Electrical conductivity

Electrical resistance measurements were performed using four probes and a Lakeshore 370 resistance bridge. A digital multimeter (Keithley 2000) monitored the temperature measured by a type K thermocouple positioned close to the sample. Bar samples, cut from cylindrical pellets, with Ag contact pads cured at 873 K, were measured in both static air and a mixture containing 4% H_2 balanced with Ar (4%H_2–Ar), from room temperature up to 1073 K during heating and cooling (3 K min^{-1}).

Fuel cell testing

Electrolyte-supported single cells were fabricated using 8 mol % yttria-stabilized zirconia (YSZ, Tosoh, Japan) cylindrical substrates, sintered at 1873 K, with 18 mm diameter and 0.5 mm thickness. Two configurations of electrolyte supported cells were studied, as illustrated in Fig. 1.

The first one was the conventional electrolyte-supported fuel cell configuration (cathode/electrolyte/anode) in which the Ni/GDC was used as the outer layer of the anode. In the conventional electrolyte-supported configuration, double layer anodes comprised of a Ni/YSZ (40/60 vol.%) functional layer at the interface with the electrolyte and the Ni/GDC current collector layer were deposited onto the YSZ support. The second configuration was the fuel cell with a catalytic layer (CFC - cathode/electrolyte/anode/catalyst) [32,33]. In CFC configuration, the Ni/GDC (18 wt% Ni) layer was deposited onto the Ni/YSZ functional (40/60 vol.%) and current collector layers (60/40 vol.%) to act as a catalytic layer avoiding direct contact of the fuel with the Ni/YSZ anode [32–34]. In both single cell configurations $La_{0.65}Sr_{0.3}MnO_3$ (LSM) cathodes were deposited over a functional composite YSZ/LSM layer deposited onto the electrolyte. Electrode layers were deposited by spin-coating using suspensions based on terpineol and ethyl cellulose. After the deposition of each electrode, a heat treatment at 1073 K for organics removal was followed by sintering at 1673 K and 1423 K for the anode and cathode, respectively. The Ni/GDC catalytic layer in the CFC single cells was deposited by spin coating after sintering of the electrodes, followed by heat treatment at 1173 K. Au and Pt mesh current collectors were attached, using the corresponding metal ink, to the surfaces of the anode and cathode, respectively, and cured at 1073 K. Single cells with active electrode area of 0.78 cm^2 were sealed on the extremity of an alumina tube sample holder, with the anode side facing the inner part of the tube, by using Aremco 552 cement. The sample holder (alumina tube and single cell) was inserted into a resistive horizontal tube furnace and connected to the metallic heads of a homemade test station with 4 Pt wires for electrical contacts. The conventional single cell was heated up to 1123 K under hydrogen (3 vol.% H_2O) and polarization measurements were carried out. At 1123 K, the fuel cell was polarized at 0.7 V and hydrogen was switched to dry ethanol carried by flowing N_2. Ethanol was gasified by bubbling N_2 through a saturator containing anhydrous ethanol at ~323 K, resulting in a gas composition of 32% of ethanol in nitrogen. The system was kept under load (0.7 V) and polarization curves were collected after 0.5 h, 1.0 h, and 1.5 h of operation under ethanol. Tests of single cell CFC were performed by heating the sample up to 1123 K under hydrogen (3 vol.% H_2O). Then, the fuel cell was polarized at 0.7 V and after stabilization of the system the fuel was changed to dry ethanol (32%) carried by N_2. The single cell CFC was continuously operated for ~50 h while the current density (i) at 0.7 V was monitored as a function of the time of operation. During all fuel cell tests, synthetic air was delivered to the cathode. Gas flow rates were set to 50 mL min^{-1} by mass flow controllers and the temperature was monitored by a thermocouple placed close to the cathode side. Polarization and impedance spectroscopy measurements were performed using a Zahner IM6 potentiostat. SEM analyses of the fractured surfaces of the anode were carried out after fuel cell operation to examine possible carbon deposits.

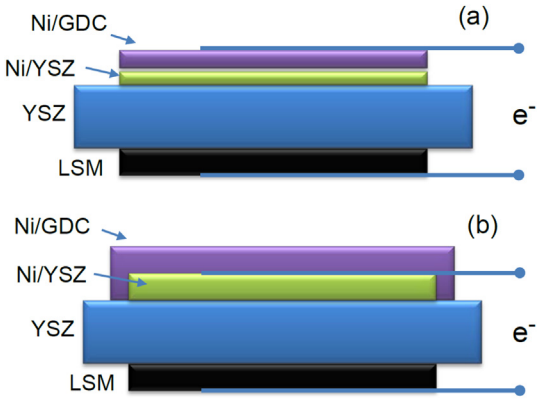

Fig. 1 – Scheme of the two solid oxide fuel cell configurations: (a) conventional electrolyte-supported single fuel cell using Ni/YSZ as the anode functional layer and Ni/GDC current collector and catalyst layer and (b) electrolyte-supported single cell having standard electrodes and a Ni/GDC catalytic layer.

Results and Discussion

Catalyst characterization

The XRD patterns of calcined and reduced samples are shown in Fig. 2. The diffractograms of calcined 18Ni/GDC and 44Ni/

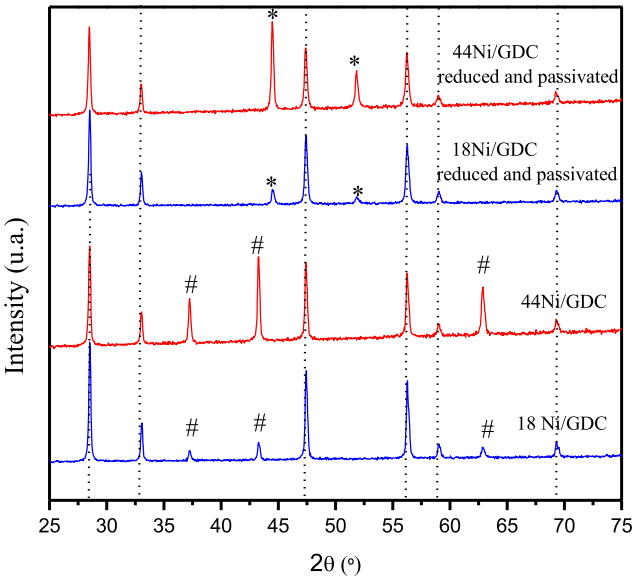

Fig. 2 – XRD patterns of calcined and reduced samples. Diffraction lines of (#) NiO; (*) Ni^0 and (——) $Ce_{0.9}Gd_{0.1}O_{1.95}$ solid solution.

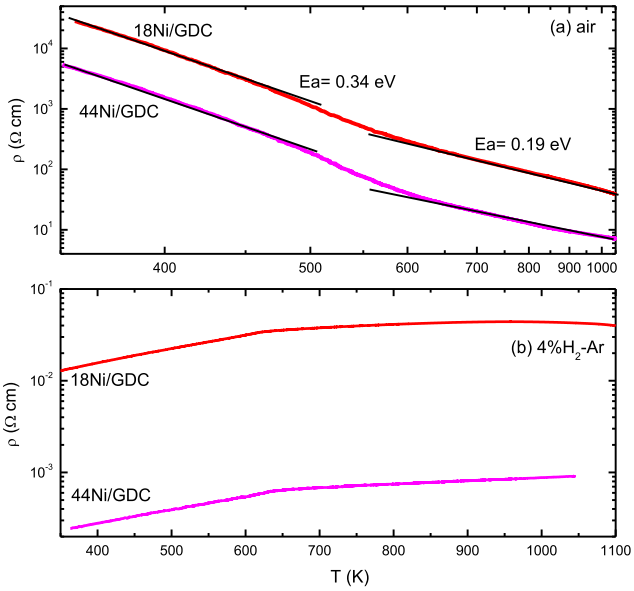

Fig. 3 – Electrical resistivity (ρ) of sintered samples as a function of temperature in (a) static air and (b) flowing 4% H_2–Ar.

GDC samples exhibited diffraction lines corresponding to a $Ce_{0.9}Gd_{0.1}O_{1.95}$ solid solution (JCPDS 75-0161) and NiO (JCPDS 24018). The reduction treatment led to the appearance of diffraction peaks attributed to metallic Ni whereas peaks corresponding to NiO were no longer observed.

Table 1 lists the crystallite sizes calculated using the Scherrer equation for both Ni/GDC samples. Increasing the Ni loading did not significantly affect the GDC and NiO crystallite sizes. The reduction treatment did not significantly change the GDC crystallite size for both Ni/GDC samples. The Ni crystallite size of 18 Ni/GDC was slightly smaller than that of 44 Ni/GDC.

The electrical properties of the Ni/GDC catalysts were investigated over a wide temperature range. The temperature dependence of the electrical resistivity (ρ) of sintered samples in both static air and flowing 4% H_2 - 96% Ar is shown in Fig. 3. Two main features are observed for the experiments carried out in air (Fig. 3(a)): i) increasing Ni content decreased ρ; and ii) both samples exhibited similar thermally activated behavior. GDC is an oxygen ion conductor with activation energy (E_a) values reported in the 0.6–1.0 eV interval, over a wide range of both temperature and oxygen partial pressure [35]. On the other hand, NiO is a p-type semiconductor, which exhibits a discontinuity in the Arrhenius plots at a temperature close to the Néel temperature (T_N ~ 250 °C) [36]. The $\rho(T)$ data in Fig 3(a) showed a clear change in slope at T ~ 250 °C in good agreement with previous reports on the electrical properties of NiO containing composites [37,38]. Both low T (T < 250 °C) and high T (T > 250 °C) ranges were fitted according to the Arrhenius equation and calculated E_a values were 0.34 eV and 0.19 eV, respectively, in agreement with previous reports [36,39]. The best fittings revealed similar E_a values for the two compositions in both temperature ranges. The observed change of slope at T ~ T_N and the calculated E_a values provide strong evidences that NiO percolated in the ceria-gadolinia matrix and controlled the charge transport of the composite.

Samples were reduced and $\rho(T)$ data were recorded in flowing 4%H_2–Ar, as shown in Fig. 3(b). The measured $\rho(T)$ resembled that of Ni, exhibiting metallic behavior for $\rho(T)$ and a characteristic change in slope at close to the Curie temperature (T_c ~ 625 K). However, as compared to Ni the magnitude of $\rho(T)$ of the cermet is shifted two orders of magnitude to higher values due to the influence of the GDC matrix. Nonetheless, such a result demonstrated that Ni percolated into the composite matrix at a volume fraction of 15 vol.% (corresponding to 18 wt.% Ni). Such a relatively low percolation threshold may be associated with the good connectivity of Ni particles in the GDC matrix, as well as with the average particle size ratio of the two phases [40]. Increasing the Ni content results in lower $\rho(T)$ and the 44Ni/GDC composite exhibited $\rho(T)$ values comparable to that of other Ni based cermets [38,41]. Such features demonstrate that the preparation method results in composites having adequate microstructural properties for both catalytic performance and electrical transport.

Table 1 – Crystallite sizes of CeO_2, NiO and metallic Ni phases calculated by Scherrer equation.

Sample	Calcined		Reduced and passivated	
	CeO_2[a] (nm)	NiO[b] (nm)	CeO_2[a] (nm)	Ni[c] (nm)
18 Ni/CeGd	41	33	39	30
44 Ni/CeGd	39	36	39	36

[a] Calculated by using the (111) ceria plane.
[b] Calculated by using the (200) NiO plane.
[c] Calculated by using the (111) metallic Ni plane.

Reactions

Ethanol conversion reactions in a fixed-bed reactor

Ethanol conversion and product distributions as a function of time on stream (TOS) for ED, SR and POX of ethanol over 18Ni/GDC catalyst at 1123 K are shown in Fig. 4. Ethanol conversion was complete and remained quite stable at all reaction conditions. Concerning product distributions, H_2, CO, and CH_4 were the main products formed for ED (Fig. 4(a)). In addition, small amounts of ethylene were also detected. These results indicate that ethanol decomposition to H_2, CO, and CH_4 and ethanol dehydration to ethylene are the reactions taking place. The addition of water to the feed (Fig. 4(b)) favored the formation of hydrogen and CO_2 and decreased the selectivity to CH_4 and CO, suggesting participation of the water-gas shift reaction. The addition of water also inhibited the formation of ethylene, indicating that SR is the main reaction taking place. These results agree very well with studies that reported an inhibiting effect of water on the dehydration of ethanol [22,23]. For POX (Fig. 4(c)), the selectivity to hydrogen decreased and the formation of CO_2 and CO increased as compared to the SR of ethanol reaction.

Fig. 5 shows the ethanol conversion and product distributions as a function of TOS for ED, SR, and POX of ethanol over 44Ni/GDC catalyst at 1123 K. The catalyst remained quite stable during 28 h, regardless of feed composition. For ED (Fig. 5(a)), H_2, CO, CH_4 and small amounts of ethylene were the products observed, which suggests that ethanol decomposition and dehydration reactions took place. The addition of water or oxygen to the feed inhibited the formation of ethylene and favored the production of CO_2.

Comparing the product distribution between 18Ni/GDC and 44Ni/GDC catalysts for the different reaction conditions provides information about the effect of metal content on the

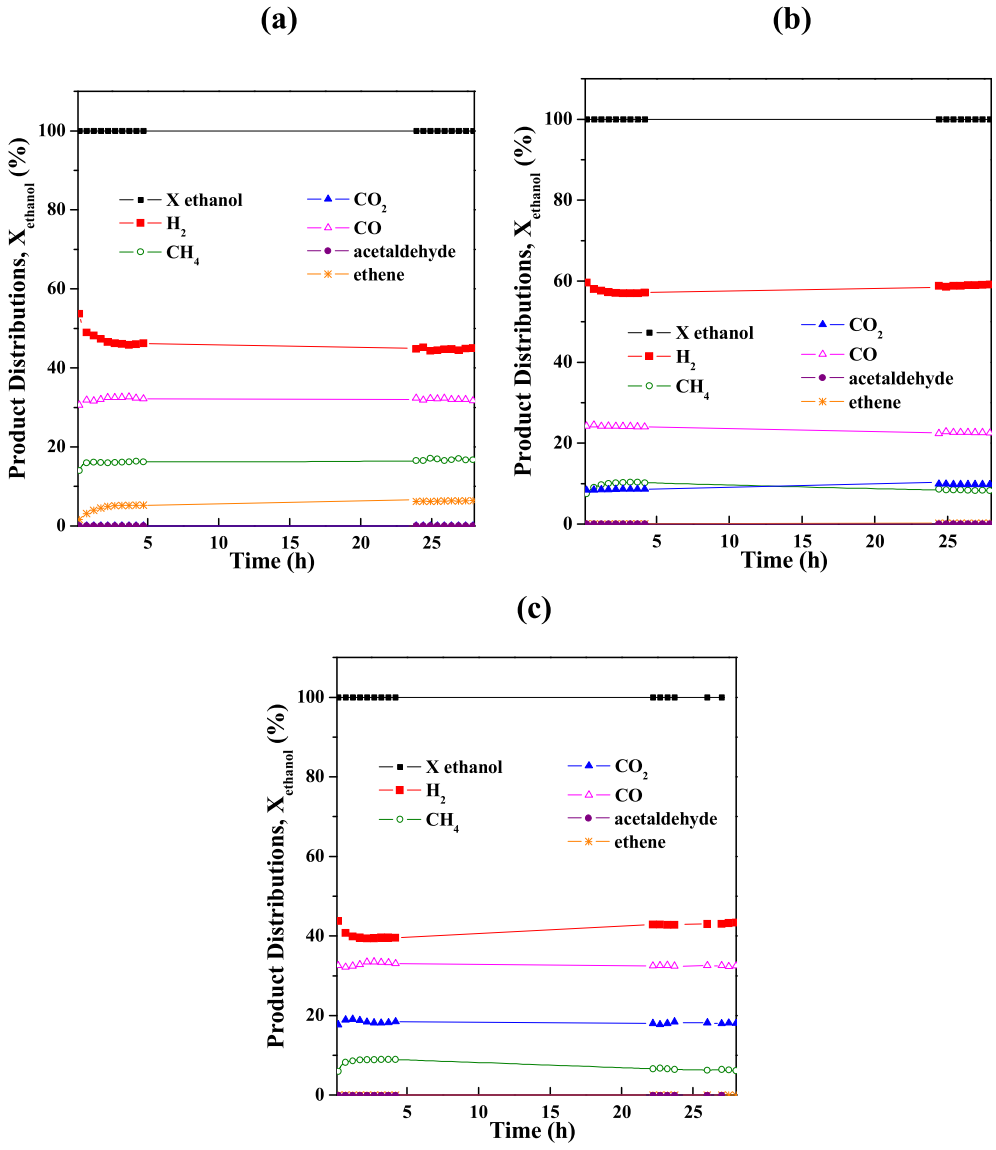

Fig. 4 – Ethanol conversion ($X_{ethanol}$) and product distributions as a function of TOS obtained over the 18 Ni/GDC catalyst at 1123 K during: (a) ED, (b) SR and (c) POX of ethanol (mass of catalyst = 20 mg; SR: H_2O/ethanol molar ratio = 3.0; POX: O_2/ethanol molar ratio = 0.5; residence time = 0.02 g s/mL).

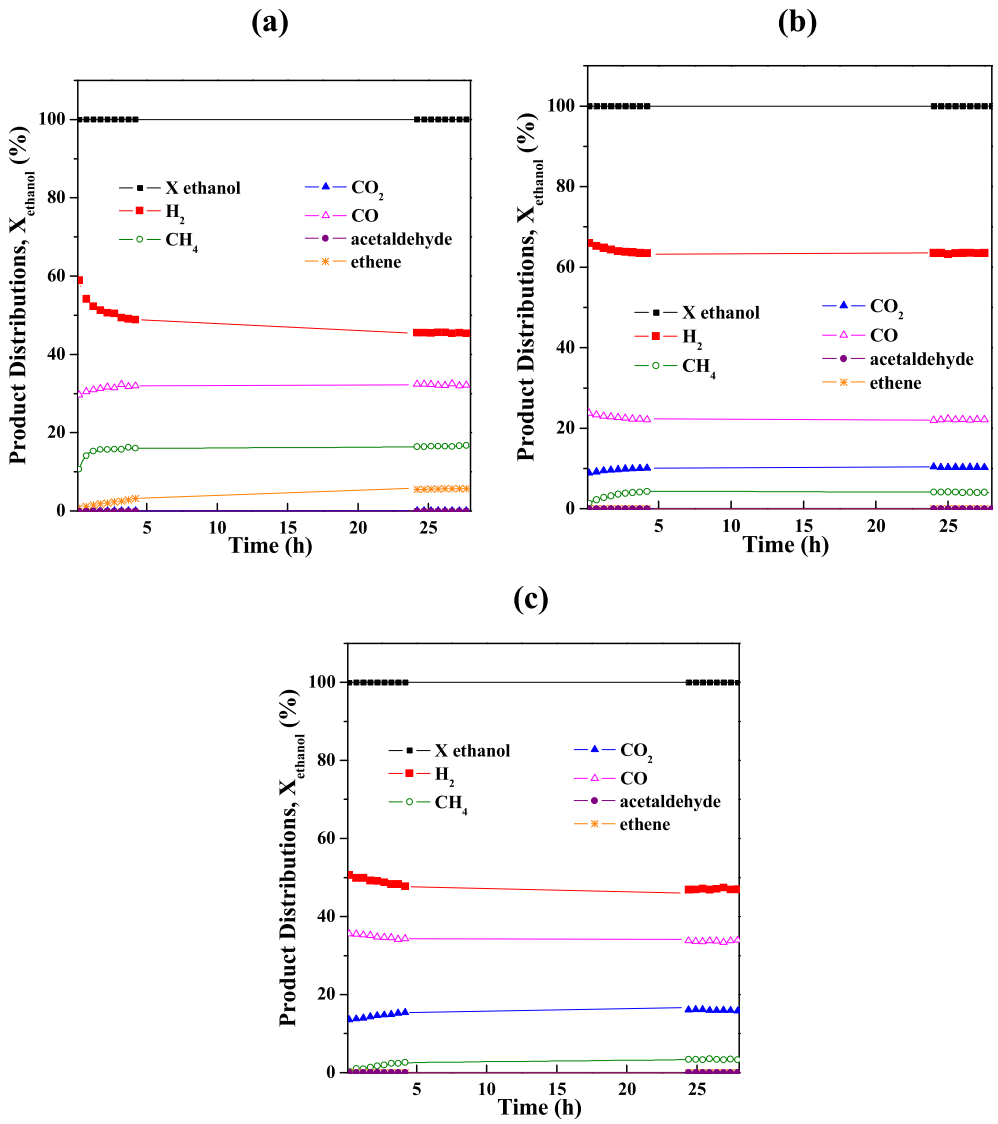

Fig. 5 – Ethanol conversion ($X_{ethanol}$) and product distributions as a function of TOS obtained over 44 Ni/GDC catalyst at 1123 K during: (a) ED, (b) SR and (c) POX of ethanol (mass of catalyst = 20 mg; SR: H_2O/ethanol molar ratio = 3.0; POX: O_2/ethanol molar ratio = 0.5; residence time = 0.02 g s/mL).

reaction pathway. Increasing the Ni content increased the hydrogen selectivity, whereas the formation of methane decreased. These results indicate that the rate of SR of methane is higher for the catalyst containing higher Ni content.

Characterization of used catalysts

SEM and TG analyses were carried out to characterize post-reaction catalysts. Fig. 6 shows the SEM micrographs of the 18Ni/GDC catalyst after ethanol conversion reactions at 1123 K. SEM images after ED revealed the formation of carbon filaments, which were no longer detected during SR or POX. The addition of water as well as oxygen thus inhibited the formation of carbon filaments.

SEM micrographs of the 44Ni/GDC catalyst after ED, SR, and POX at 1123 K are shown in Fig. 7. Carbon filaments were only observed after ED and they were not detected after SR or POX, similar to the results obtained for the catalyst with lower Ni loading.

Fig. 8 displays the TPO profiles of 18Ni/GDC and 44Ni/GDC after ED, SR and POX at 1123 K, respectively. For both catalysts, peaks were only detected on the TPO profiles after ED. The TPO profile of 18Ni/GDC catalyst exhibited one peak at 931 K whereas a peak at 912 K and a shoulder at 1035 K were observed for the 44Ni/GDC catalyst. According to previous reports [42–46], CO_2 peaks in the low temperature region (<673 K) were related to oxidation of amorphous carbon overlaying the metal surface. On the other hand, the CO_2 formed at high temperatures was assigned to filamentous (773–973 K) and graphitic carbon (>973 K). Therefore, the TPO profiles after carrying out ED reaction indicate oxidation of filamentous and graphitic carbon for both samples.

From the TPO profiles, the amount of carbon deposited on Ni/GDC catalysts after ED, SR, and POX at 1123 K was

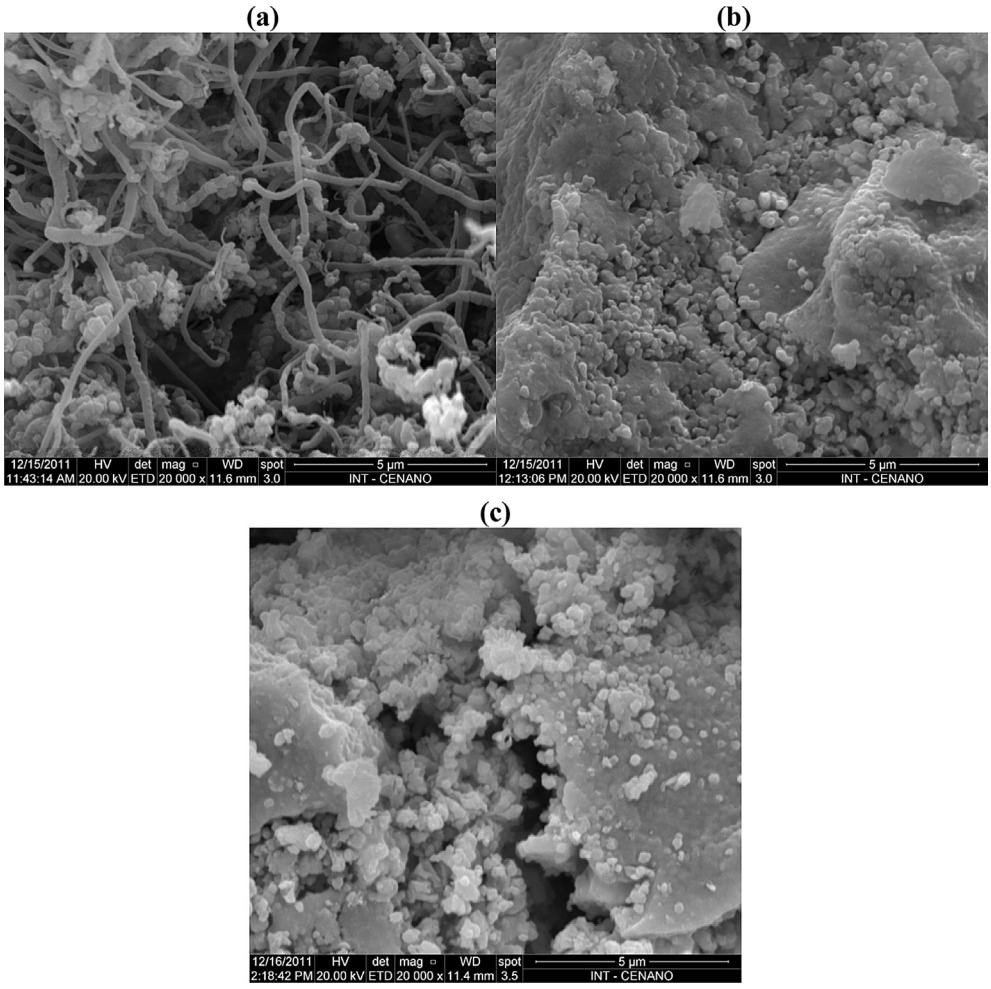

Fig. 6 – SEM micrographs of the 18Ni/GDC catalyst after: (a) ED; (b) SR and (c) POX reaction tests. (Reaction temperature: 1123 K; mass of catalyst = 20 mg; SR: H_2O/ethanol molar ratio = 3.0; POX: O_2/ethanol molar ratio = 0.5; residence time = 0.02 g s/mL).

calculated. A large amount of carbon was deposited during ED over both Ni/GDC catalysts. However, the amount of carbon deposited over 44Ni/GDC catalyst (3.9 $mg_{carbon}/(g_{catalyst}{}^{*}h)$) was 3-fold higher than that observed for the 18Ni/GDC catalyst (12.5 $mg_{carbon}/(g_{catalyst}{}^{*}h)$). The addition of water or oxygen to the feed suppressed the formation of carbon during SR and POX at 1123 K. Adding water or oxygen to the feed promotes the gasification of carbon and this, in turn, decreases the catalyst deactivation rate through continuous carbon removal.

Single cell tests

In order to investigate both the electrical and catalytic properties of the Ni/GDC anodes in ethanol-fueled SOFC, two types of single cells (Fig. 1) using the ceria-based cermet were fabricated and tested at 1123 K: i) the conventional electrolyte-supported fuel cell configuration and ii) the catalytic layer configuration (CFC). The main point of measuring these two single cell configurations is to evaluate separately the influence of the electrical conductivity and the catalytic properties for stable fuel cell performance on direct ethanol.

i) Conventional electrolyte-supported fuel cell

In this configuration, electrolyte-supported single cells (cathode/electrolyte/anode) were tested using Ni/GDC used as the outer anode layer (current collector). The measured polarization (I–V) curves are shown in Fig. 9 for both samples 18Ni/GDC (Fig. 9(a)) and 44Ni/GDC (Fig. 9(b)).

Both samples exhibited OCV of ~1 V under H_2 (3 vol.% H_2O), a value compatible with the expected thermodynamic potential for the humidified hydrogen oxidation reaction. The measured polarization curves were quite linear in the investigated range, suggesting that the ohmic drop associated with the thick electrolyte support is the most significant contribution. Single cells with higher Ni content displayed a slightly higher maximum power density under H_2 than those with lower metal content, a feature possibly related to the higher electrical conductivity of the 44Ni/GDC sample (Fig. 3).

When H_2 was switched to dry ethanol, the anodes with 18 and 44 wt.% of Ni exhibited similar behavior. As compared to H_2, both samples showed linear polarization curves with practically unchanged OCV. In fact, as hydrogen was observed

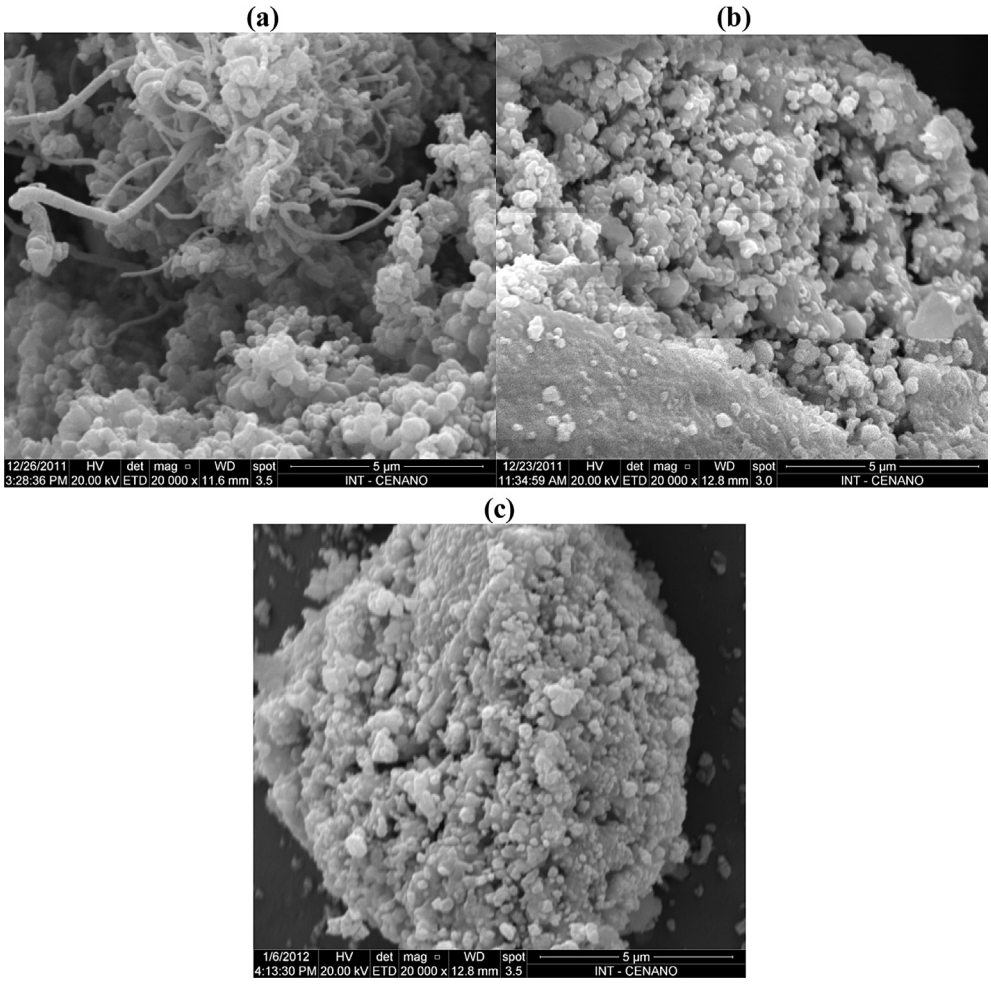

Fig. 7 – SEM micrographs of the 44Ni/GDC catalyst after: (a) ED; (b) SR and (c) POX. (Reaction temperature: 1123 K; mass of catalyst = 20 mg; SR: H_2O/ethanol molar ratio = 3.0; POX: O_2/ethanol molar ratio = 0.5; residence time = 0.02 g s/mL).

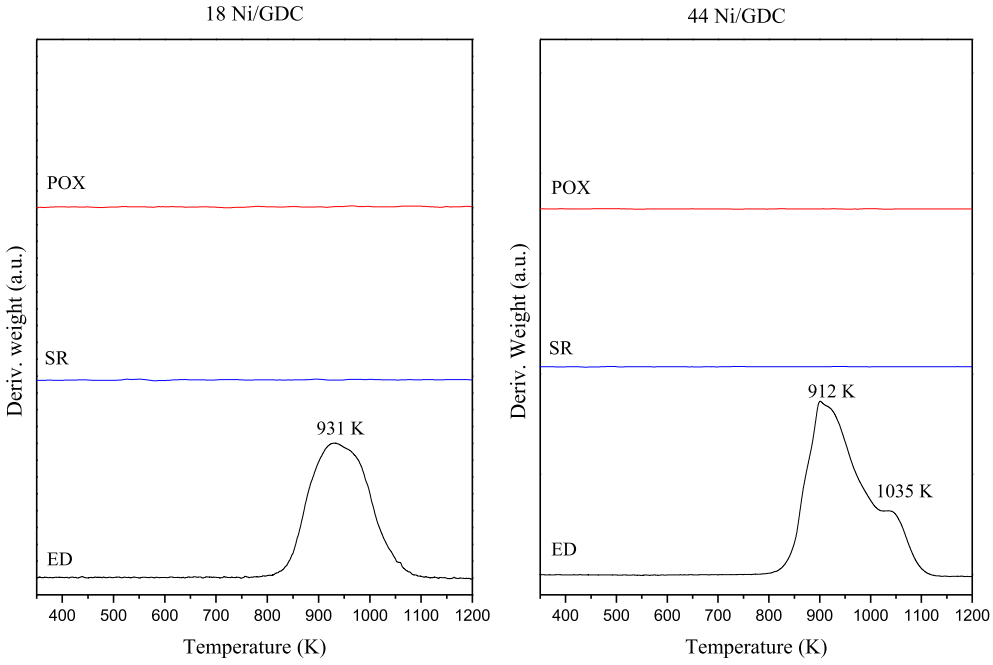

Fig. 8 – TPO profiles of 18Ni/GDC and 44Ni/GDC catalysts after ED, SR and POX reaction tests at 1123 K.

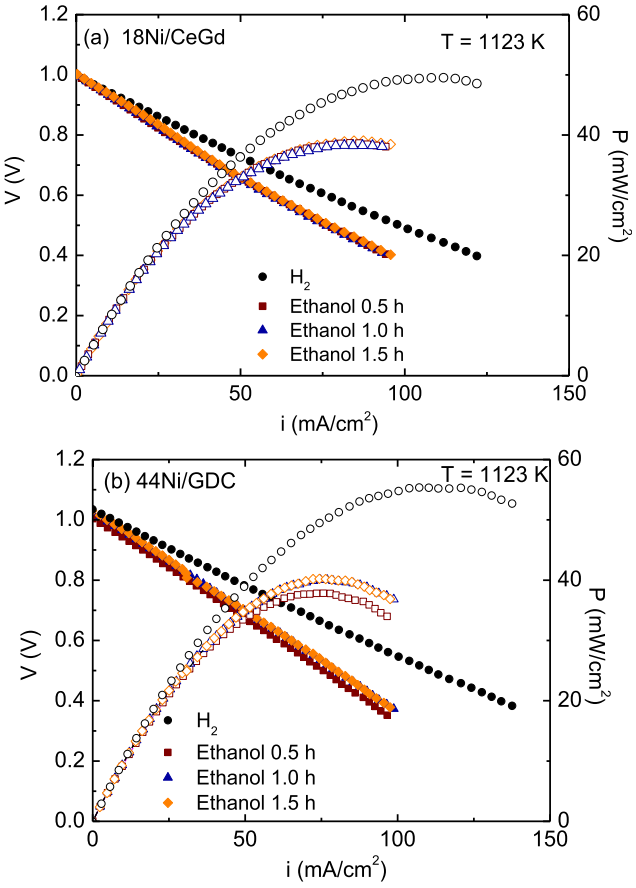

Fig. 9 – Polarization curves of single SOFC obtained at 1123 K using H_2 and ethanol feeds with (a) 18Ni/GDC and (b) 44Ni/GDC as anodes.

to be the main product of the catalytic decomposition of ethanol for the Ni/GDC anodes (Figs. 4 and 5), it is expected that the main reaction taking place at the electrolyte/anode interface is the electrochemical oxidation of hydrogen, thus maintaining the OCV at values close to 1 V. However, as compared to hydrogen, a decrease in the maximum power density occurred when the fuel cell was fed with dry ethanol. This result can be related to either: i) a fuel dilution, since ethanol was found to be converted to ~60% of H_2 in the ceria-based catalyst (Figs. 4 and 5) or ii) a small decrease of the local temperature due to the endothermic character of the ethanol reforming reaction. It is interesting to note that under dry ethanol both anodes behaved in a similar manner, indicating that, independently of the higher conductivity of the 44Ni/GDC, the performance of the single cells was not controlled by the electrical conductivity of the anode.

A limited number of studies on ethanol fueled SOFC using ceria-based anodes are reported in the literature, only few of them investigated direct ethanol (without adding water/steam) and stability tests are rarely found. The wide range of experimental parameters for both fuel cell fabrication and testing makes any direct comparison practically impossible. In our work, maximum power densities in Fig. 9 were rather low, but compatible to the ones obtained for electrolyte supported fuel cells operating under dry ethanol [12–15,17]. Higher values of power densities were reported for single cells using a catalytic layer for direct ethanol operation. Furthermore, studies reporting on SOFC that operate with ethanol and steam mixtures usually display higher power densities [6,8–11,24]. This is probably due to the higher amount of hydrogen produced by the steam reforming reaction in comparison to direct ethanol conversion (eqs. (3) and (4)). Nevertheless, important future improvements of the anodes are required including microstructural optimization for testing high power output fuel cells with ceria-based anodes for direct ethanol SOFCs.

$$C_2H_5OH + 3H_2O \rightarrow 6H_2 + 2CO_2 \quad (3)$$

$$C_2H_5OH \rightarrow H_2 + CO + CH_4 \quad (4)$$

Impedance diagrams of the single cells measured at OCV in both hydrogen and ethanol are shown in Fig. 10. Both samples exhibited impedance diagrams with at least two main polarization components. For 18Ni/GDC both the ohmic and polarization resistances are considerably higher than the one of 44Ni/GDC, in accordance with the lower Ni content. Moreover, the electrode polarization was found to be significant and reflects the non-optimized anode microstructure. Under ethanol, as compared to H_2, samples had increased ohmic resistance, but comparable electrode polarization, which resulted in slightly increased total resistance for both anodes.

Concerning anode stability, the practically coincident polarization curves taken after 0.5, 1.0, and 1.5 h (Fig. 9) of operation on dry ethanol indicate good short term stability of the fuel cells. This result suggests that significant carbon deposition did not occur during operation of the single cell. To investigate possible carbon formation, the anodes of tested single cells were analyzed by SEM after the operation on ethanol. Fig. 11 shows cross sectional images of the anode with 44 Ni/GDC. Careful analyses showed no evidence of relevant carbon deposits in the anode layer.

The electrochemical tests carried out do not clarify whether the similar performance in ethanol for both anodes with different Ni volume fractions is related to the catalytic

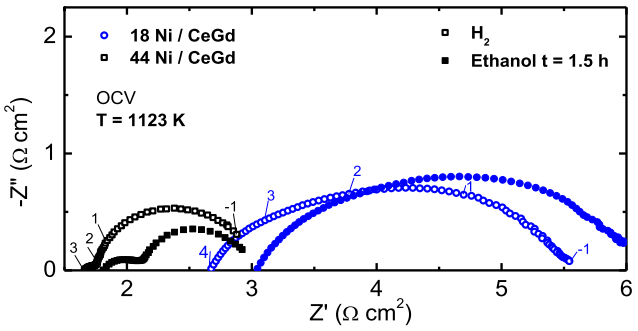

Fig. 10 – Impedance spectroscopy diagrams at OCV for electrolyte-supported single cells using Ni/GDC anode running in hydrogen and ethanol. Numbers indicate the logarithm of measuring frequency.

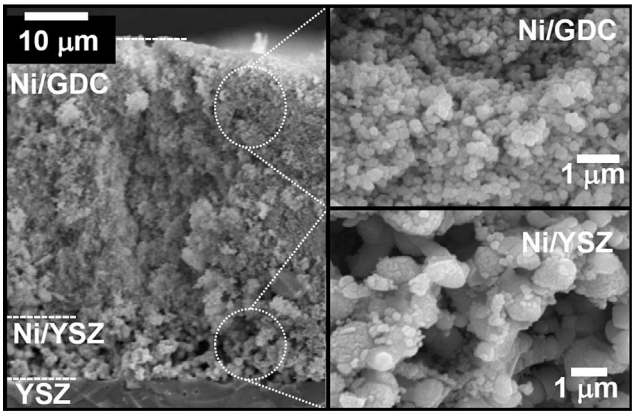

Fig. 11 – Scanning electron microscopy of fractured cross sections of the anode of single cells (SFC) tested for direct ethanol conversion. The inset shows higher magnification images of the indicated layers.

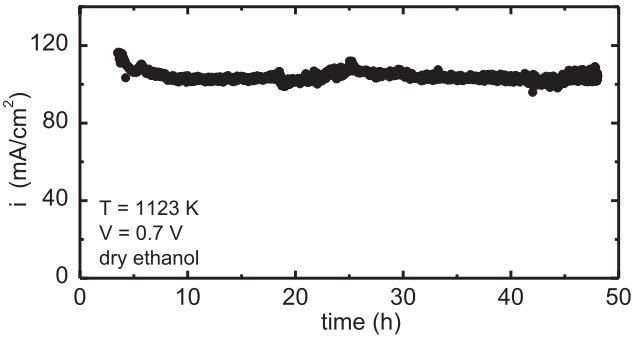

Fig. 12 – Current density at 0.7 V as a function of the operation time of the fuel cell with 18Ni/GDC catalytic layer running on dry ethanol at 1123 K for direct conversion.

and transport properties or to possible limitations due to microstructural (porosity, grain size, pore size distribution, etc.). Such parameters are expected to play a major role in single cells with relatively thin anodes and low current outputs. In the conventional fuel cell configuration, the Ni/GDC layer performs simultaneously two functions as the current collector anode layer and the catalytic layer that converts ethanol to hydrogen. Therefore, in order to have a better assessment of the role of the Ni/GDC cermet, single cells using a catalytic layer were investigated for direct ethanol operation over long periods of time.

ii) Fuel cell with catalytic layer (CFC)

In the CFC configuration (cathode/electrolyte/anode/catalyst) the transport properties of the catalytic layer is irrelevant because current collection is made over the Ni/YSZ anode (Fig. 1). Thus, the electrochemical tests of CFC configuration were performed with the cermet with the lowest Ni content (18 wt.%) by depositing it as an extra layer onto the anode of the conventional single cell. Such a layer acts both as a catalyst to convert ethanol and a barrier to avoid direct contact between the fuel and the Ni/YSZ anode [16,17,32–34]. The main idea of studying the CFC configuration was to analyze the stability during continuous operation and to evaluate the operation mechanism using dry ethanol as the fuel. The operation mechanism taking place in direct ethanol CFC is the gradual internal reforming in which the catalytic and electrochemical reactions occur into different layers [16,17,19,32–34].

The current density at 0.7 V of the CFC running on dry ethanol at 1123 K was recorded as a function of operation time, as shown in Fig. 12. It is possible to estimate the power density of this fuel cell at 0.7 V to be approximately 70 mW/cm^2. This value is almost twice larger than that of the conventional electrolyte-supported fuel cell (Fig. 9). This results from the fact that we used the standard anode Ni/YSZ with optimized microstructural properties instead of the Ni/GDC layer. However, as the main point of using the catalytic layer was to provide evidence of the catalytic effectiveness of the Ni/GDC layer, we have focused on measuring the stability of the fuel cell (Fig. 11) rather than performance. After stabilization during the initial hours of operation, the fuel cell exhibited remarkable stability during the test (~50 h). This is a strong indication that Ni/GDC catalysts are stable under the operating conditions of SOFCs. This improved stability is associated with the resistance to carbon formation.

The impedance diagrams taken at 0.7 V along the stability test under ethanol are shown in Fig. 13. Impedance diagrams were found to be described by a semicircle at the high-frequency (10^3–10^2 Hz) and a spike at the low frequency (<1 Hz) end. Such a spike at low-frequency can be related to the catalytic layer that possibly induces some mass transfer impedance, as previously reported [16,17]. It can be observed that the ohmic resistance slightly increased in the initial hours of test, whereas the polarization resistance increased more pronouncedly for testing times longer than 25.5 h. However, the absence of a completely defined low frequency semicircle arc makes difficult to evaluate the total polarization resistance of the fuel cell. Nonetheless, such a polarization increase suggests an electrochemical degradation of the fuel cell, which was not optimized for long periods of operation, rather than degradation due to carbon formation. Previous data showed that significant amounts of

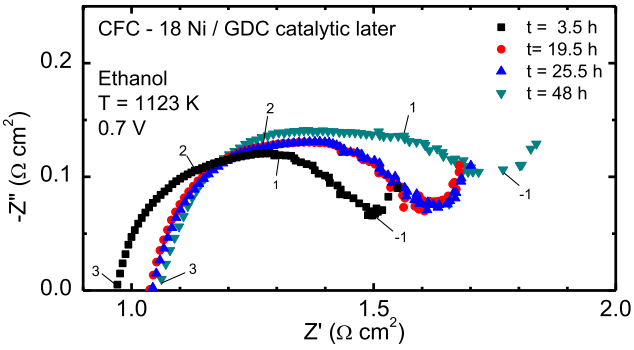

Fig. 13 – Impedance spectroscopy diagrams measured at 0.7 V during stability test in ethanol of single cell using Ni/GDC catalytic layer over the anode. Numbers indicate the logarithm of measuring frequency.

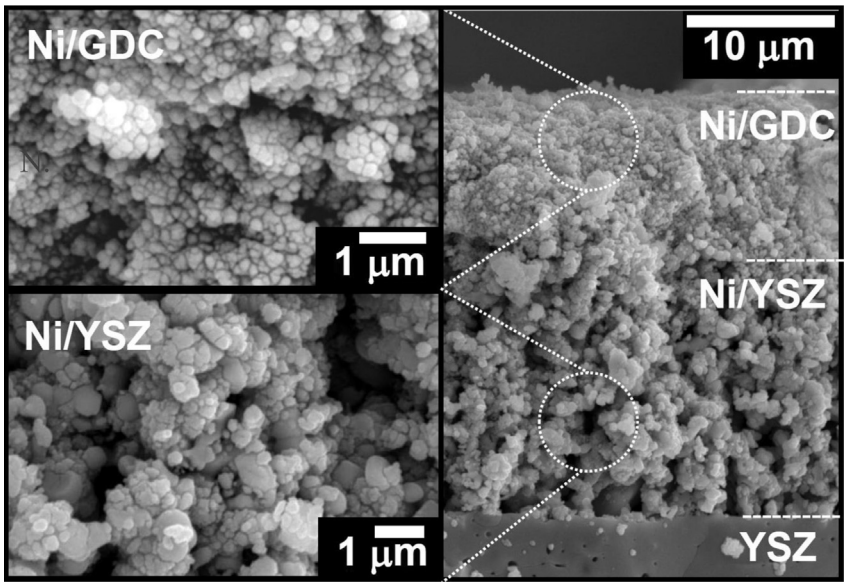

Fig. 14 – –Scanning electron microscopy of fractured cross sections of the anode of single cells (CFC) tested for direct ethanol conversion. The inset shows higher magnification images of the indicated layers.

carbon deposits are formed over Ni/YSZ much faster than the time interval measured in Fig. 12 resulting in a marked degradation of the performance of the fuel cell [47,48].

The good stability of the single cells CFC running on anhydrous ethanol is attributed to both the catalytic properties of Ni/GDC and the gradual internal reforming of ethanol, as previously reported [16–17]. Gradual internal reforming has been studied in detail being experimentally and theoretically demonstrated in some recent studies [16,17,19,32–34]. This mechanism is based on a local decoupling between the steam reforming of the fuel in the catalytic layer and the electrochemical oxidation of hydrogen, which takes place at the anode/electrolyte triple-phase boundary. Thus, the water released by the electrochemical oxidation of hydrogen at the anode (eq. (5)) is used for the ethanol steam reforming (eq. (6)) in the Ni/GDC layer [16,17,32–34]. Ideally, such a mechanism can be represented by the following reaction scheme:

$$H_2 + O^{2-} \rightarrow H_2O + 2e^- \quad (5)$$

$$C_2H_5OH + 3H_2O \rightarrow 2CO_2 + 6H_2 \quad (6)$$

Therefore, provided that an efficient catalyst is used, reactions (5) and (6) sustain each other and ensure stable fuel cell operation on dry ethanol, as demonstrated by the tests shown in Fig. 12. Such mechanism is difficult to be directly inferred and more complex reactions possibly take place during the direct ethanol SOFC operation [19]. Nevertheless, the main experimental evidence supporting such mechanism is shown in Fig. 11. It is important to consider that no steam is added to the fuel, and only the steam produced by the electrochemical reactions in the (Ni/YSZ) anode/(YSZ) electrolyte interface is available for the reforming in the Ni/GDC catalytic layer. This result is corroborated by the catalytic tests in fixed-bed reactor. They clearly demonstrated that no carbon is formed for SR of ethanol over Ni/GDC whereas for the ethanol decomposition (no water added) carbon deposits were detected. The electrochemical and catalytic properties of Ni/YSZ are indeed well-established and one of the best known for hydrogen. However, it is also well-known that the Ni/YSZ anode cannot sustain the operation under carbon-containing fuels. Under such fuels, the Ni/YSZ anode (without added water) rapidly collapses due to severe carbon formation. Therefore, our results are a strong indication that the Ni/GDC cermet is the active catalyst layer that ensures ethanol conversion for the stable operation of the fuel cell. Thus, if the gradual internal reforming would not be in operation one should expect the fuel cell running without any added water to collapse within few hours of operation, as it is usually observed in many studies. However, Fig. 11 shows a fuel cell running for 50 h without any significant degradation, giving strong indication that no carbon is formed, thus supporting the gradual internal reforming as the mechanisms controlling the operation of the direct ethanol SOFC with Ni/GDC catalytic layer. Therefore, the main advantage of this configuration, as demonstrated in Fig. 11, is the possibility to operate a direct ethanol fuel cell without adding water to the fuel.

The direct ethanol fuel cells were analyzed after stability tests to further investigate possible carbon deposits. The SEM image of the cross section of the anode shown in Fig. 14 did not reveal any carbon deposits in the anode layers. Such result is in agreement with previous data on fuel cells operating at even longer times, but using iridium/GDC as the catalyst [16,17]. Thus, the present data is a strong indication that the gradual internal reforming of ethanol is viable when a non-precious metal catalyst is used.

It is important to consider that most of the studies on ethanol fueled SOFC have relied on ethanol/steam mixtures as the fuel and only a very limited number of studies have presented short term stability data [12]. In the present study, the single cells showed good stability when fed directly with dry

ethanol, which was attributed to the absence of carbon deposits. Usually, performance degradation due to carbon formation has been reported to be pronounced and to occur within the first minutes of operation of standard Ni-based cermet anodes fed directly with dry carbon-containing fuels [47,48]. Therefore, based on the catalytic tests (Figs. 4 and 5), the absence of carbon formation during fuel cell operation suggests that the SR of ethanol takes place at the anode, since carbon deposition occurred in the ED reaction. In fact, water produced by the electrochemical reaction (eq. (5)) is in excess for the catalytic reforming reaction (eq. (6)) that promotes carbon removal and inhibits catalyst deactivation. Such a result evidences that fuel cell performance observed is attributed to the stable and efficient catalytic properties of the Ni/GDC cermet and the operating mechanism of gradual internal reforming [16,17,19,32–34].

Conclusions

The catalytic tests performed in a fixed-bed reactor showed that a large amount of carbon was formed over both Ni/GDC catalysts under dry ethanol feed. In addition, increasing Ni content increased the amount of carbon deposited. This was likely due to the larger Ni particle size of the sample containing 44 wt.% of Ni. However, the addition of water or oxygen to the feed inhibited the formation of carbon during SR and POX at 1123 K for both samples. The results obtained for fuel cells operating with dry ethanol indicate that there is no carbon formation on the Ni/GDC anodes. This result was attributed to the catalytic properties of the Ni/GDC catalyst and the gradual internal reforming mechanism, which provides the necessary water for the fuel reforming in the anode catalytic layer.

Acknowledgments

One of the authors (Bruno Lobato Augusto) acknowledges a scholarship received from CAPES. The authors are grateful for support from the Brazilian agencies CNPq and FINEP.

REFERENCES

[1] Laosiripojana N, Assabumrungrat S. Catalytic steam reforming of methane, methanol, and ethanol over Ni/YSZ: the possible use of these fuels in internal reforming SOFC. J Power Sources 2007;163:943–51.
[2] Suna C, Stimming U. Recent anode advances in solid oxide fuel cells. J Power Sources 2007;171:247–60.
[3] Tsiakarasa P, Demin A. Thermodynamic analysis of a solid oxide fuel cell system fuelled by ethanol. J Power Sources 2001;102:210–7.
[4] Douvartzides SL, Coutelieris FA, Demin AK, Tsiakaras PE. Electricity from ethanol fed SOFCs: the expectations for sustainable development and technological benefits. Int J Hydrogen Energy 2004;29:375–9.
[5] Arpornwichanop A, Chalermpanchai N, Patcharavorachot Y, Assabumrungrat S, Tade M. Performance of an anode-supported solid oxide fuel cell with direct-internal reforming of ethanol. Int J Hydrogen Energy 2009;34:7780–8.
[6] Ye XF, Wang SR, Wang ZR, Xiong L, Sun XF, Wen TL. Use of a catalyst layer for anode-supported SOFCs running on ethanol fuel. J Power Sources 2008;177:419–25.
[7] Ye XF, Wang SR, Hu Q, Wang ZR, Wen TL, Wen ZY. Improvement of multi-layer anode for direct ethanol solid oxide fuel cells. Electrochem Commun 2009;11:823–6.
[8] Huang B, Wang SR, Liu RZ, Wen TL. Preparation and performance characterization of the Fe–Ni/ScSZ cermet anode for oxidation of ethanol fuel in SOFCs. J Power Sources 2007;167:288–94.
[9] Ye XF, Huang B, Wang SR, Wang ZR, Xiong L, Wen TL. Preparation and performance of a Cu–CeO_2–ScSZ composite anode for SOFCs running on ethanol fuel. J Power Sources 2007;164:203–9.
[10] Huang B, Wang SR, Liu RZ, Ye XF, Nie HW, Sun XF, et al. Performance of $La_{0.75}Sr_{0.25}Cr_{0.5}Mn_{0.5}O_3-\delta$ perovskite-structure anode material at lanthanum gallate electrolyte for IT-SOFC running on ethanol fuel. J Power Sources 2007;167:39–46.
[11] Huang B, Zhu XJ, Hu WQ, Wang YY, Yu QC. Characterization of the Ni–ScSZ anode with a LSCM–CeO_2 catalyst layer in thin film solid oxide fuel cell running on ethanol fuel. J Power Sources 2010;195:3053–9.
[12] Armstrong EN, Park J, Minh NQ. High-performance direct ethanol solid oxide fuel cells. Electrochem Solid State Lett 2012;15:B75–7.
[13] Muccillo R, Muccillo ENS, Fonseca FC, de Florio DZ. Characteristics and performance of electrolyte-supported solid oxide fuel cells under ethanol and hydrogen. J Electrochem Soc 2008;155:B232–5.
[14] Cimenti M, Hill JM. Direct utilization of methanol and ethanol in solid oxide fuel cells using Cu–Co(Ru)/$Zr_{0.35}Ce_{0.65}O_2-\delta$ anodes. J Power Sources 2010;195:3996–4001.
[15] Jiang SP, Ye Y, He T, Ho SB. Nanostructured palladium–$La_{0.75}Sr_{0.25}Cr_{0.5}Mn_{0.5}O_3/Y_2O_3$–$ZrO_2$ composite anodes for direct methane and ethanol solid oxide fuel cells. J Power Sources 2008;185:179–82.
[16] Nobrega SD, Galesco MV, Girona K, Florio DZ, Steil MC, Georges S, et al. Direct ethanol solid oxide fuel cell operating in gradual internal reforming. J Power Sources 2012;213:156–9.
[17] Nobrega SD, Gelin P, Georges S, Steil MC, Augusto BL, Noronha FB, et al. A fuel-flexible solid oxide fuel cell operating in gradual internal reforming. J Electrochem Soc 2014;161:F354–9.
[18] Minh NQ. Ceramic fuel cells. J Am Ceram Soc 1993;76:563–88.
[19] Atkinson A, Barnett S, Gorte RJ, Irvine JTS, Mcevoy AJ, Mogensen M, et al. Advanced anodes for high-temperature fuel cells. Nat Mater 2004;3:17–27.
[20] Park S, Vohs JM, Gorte RJ. Direct oxidation of hydrocarbons in a solid-oxide fuel cell. Nature 2000;404:265–7.
[21] Augusto BL, da Costa LOO, Noronha FB, Colman RC, Mattos LV. Ethanol reforming over Ni/CeGd catalysts with low Ni content. Int J Hydrogen Energy 2012;37:12258–70.
[22] Mattos LV, Jacobs G, Davis BH, Noronha FB. Production of hydrogen from ethanol: review of reaction mechanism and catalyst deactivation. Chem Rev 2012;112:4094–123.
[23] Laosiripojana N, Assabumrungrat S, Charojrochkul S. Steam reforming of ethanol with co-fed oxygen and hydrogen over Ni on high surface area ceria support. Appl Catal A Gen; 2007:180–8.
[24] Ye XF, Wang SR, Hu Q, Chen JY, Wen TL, Wen ZY. Improvement of Cu–CeO_2 anodes for SOFCs running on ethanol fuels. Solid State Ionics 2009;180:276–81.
[25] Fonseca FC, Uhlenbruck S, Nedéléc R, Buchkremer HP. Properties of bias-assisted sputtered gadolinia-doped ceria

interlayers for solid oxide fuel cells. J Power Sources 2010;195:1599–604.
[26] Rocha RA, Muccillo ENS. Efeito da temperatura de calcinação e do teor de dopante nas propriedades físicas da céria-gadolínia preparada pela complexação de cátions com ácido cítrico. Ceramica 2001;47:219–24.
[27] Song H, Ozkan US. Ethanol steam reforming over co-based catalysts: role of oxygen mobility. J Catal 2009;261:66–74.
[28] da Silva AM, de Souza KR, Mattos LV, Jacobs G, Davis BH, Noronha FB. The effect of support reducibility on the stability of Co/CeO_2 for the oxidative steam reforming of ethanol. Catal Today 2011;164:234–9.
[29] Rostrup-Nielsen JR, Sehested J, Norskov J. Hydrogen and synthesis gas by steam- and CO_2 reforming. Adv Catal 2002;47:65–139.
[30] Modafferi V, Panzera G, Baglio V, Frusteri F, Antonucci PL. Propane reforming on Ni–Ru/GDC catalyst: H_2 production for IT-SOFCs under SR and ATR conditions. Appl Catal A Gen 2008;334:1–9.
[31] Jasinski P, Suzuki T, Petrovsky V, Andersonb HU. Nanocomposite nickel ceria cermet with low nickel content for anode-supported SOFCs. Electrochem Solid State Lett 2005;8:A219–21.
[32] Klein JM, Hénault M, Roux C, Bultel Y, Georges S. Direct methane solid oxide fuel cell working by gradual internal steam reforming: analysis of operation. J Power Sources 2009;193:331–7.
[33] Klein JM, Hénault M, Gélin P, Bultel Y, Georges S. A solid oxide fuel cell operating in gradual internal reforming conditions under pure dry methane. Electrochem Solid State Lett 2008;11:B144–7.
[34] Klein JM, Georges S, Bultel Y. Modeling of a SOFC fueled by methane: anode barrier to allow gradual internal reforming without coking. J Electrochem Soc 2008;155:B333–9.
[35] Mogensen M, Sammes NM, Tompsett GA. Physical, chemical and electrochemical properties of pure and doped ceria. Solid States Ion 2000;129:63–94.
[36] Vernon MW, Lovell MC. Anomalies in the electrical conductivity of nickel oxide above room temperature. J Phys Chem Solids 1966;27:1125–31.
[37] Esposito V, de Florio DZ, Fonseca FC, Muccillo ENS, Muccillo R, Traversa E. Electrical properties of YSZ/NiO composites prepared by a liquid mixture technique. J Eur Ceram Soc 2005;25:2637–41.
[38] Fonseca FC, de Florio DZ, Esposito V, Traversa E, Muccillo ENS, Muccillo R. Mixed ionic–electronic YSZ/Ni composite for SOFC anodes with high electrical conductivity. J Electrochem Soc 2006;153:A354–60.
[39] Biju V, Khadar MA. AC conductivity of nanostructured nickel oxide. J Mater Sci 2001;36:5779–87.
[40] McLachlan DS, Blaszkiewicz M, Newnham RE. Electrical resistivity of composites. J Am Ceram Soc 1990;73:2187–203.
[41] Muecke UP, Graf S, Rhyner U, Gauckler LJ. Microstructure and electrical conductivity of nanocrystalline nickel- and nickel oxide/gadolinia-doped ceria thin films. Acta Mater 2008;56:677–87.
[42] Fatsikostas AN, Verykios XE. Reaction network of steam reforming of ethanol over Ni-based catalysts. J Catal 2004;225:439–52.
[43] Galetti AE, Gomez MF, Arrua LA, Abello MC. Hydrogen production by ethanol reforming over NiZnAl catalysts influence of Ce addition on carbon deposition. Appl Catal A Gen 2008;348:94–102.
[44] Sanchez-Sanchez MC, Navarro RM, Fierro JLG. Ethanol steam reforming over $Ni/M_xO_y–Al_2O_3$ (M = Ce, La, Zr and Mg) catalysts: influence of support on the hydrogen production. Int J Hydrogen Energy 2007;32:1462–71.
[45] de Lima SM, da Silva AM, da Costa LOO, Assaf JM, Jacobs G, Davis BH, et al. Evaluation of the performance of Ni/La_2O_3 catalyst prepared from $LaNiO_3$ perovskite-type oxides for the production of hydrogen through steam reforming and oxidative steam reforming of ethanol. Appl Catal A Gen 2010;377:181–90.
[46] da Costa LOO, da Silva AM, Noronha FB, Mattos LV. The study of the performance of Ni supported on gadolinium doped ceria SOFC anode on the steam reforming of ethanol. Int J Hydrogen Energy 2012;37:5930–9.
[47] Mallon C, Kendall K. Sensitivity of nickel cermet anodes to reduction conditions. J Power Sources 2005;145:154–60.
[48] Ferlauto AS, de Florio DZ, Fonseca FC, Esposito V, Muccillo R, Traversa E, et al. Chemical vapor deposition of multi-walled carbon nanotubes from nickel/yttria-stabilized zirconia catalysts. Appl Phys A 2006;84:271–6.